AIAA 99-0975

DSMC Computations of the Progress-M Spacecraft Retrofiring Exhaust Plume

J. A. Drakes and D. G. Swann
Sverdrup Technology, Inc., AEDC Group
Arnold Engineering Development Center
Arnold Air Force Base, Tennessee 37389

and

G. F. Karabadzhak and Yu. Plastinin
TsNIIMASH
Korolev, Russia

37th AIAA Aerospace Sciences Meeting & Exhibit
January 11-14, 1999 / Reno, NV

DSMC Computations of the Progress-M Spacecraft Retrofiring Exhaust Plume*

J. A. Drakes† and D. G. Swann
Sverdrup Technology, Inc., AEDC Group
Arnold Engineering Development Center
Arnold Air Force Base, TN 37389

G. F. Karabadzhak‡ and Yu. Plastinin‡
TsNIIMASH
Korolev, Russia

Abstract

A set of DSMC computations using the SOCRATES computer code has been performed to aid in the development and analysis of the MirEx experiment to observe UV radiation from spacecraft thruster plumes. The plumes of interest for this report originate from the amine propellant main engine of the Progress-M and Soyuz-TM spacecraft. The altitude of the plume observations is approximately 380 km. The SOCRATES calculations provide a baseline estimate of the spatial distribution of the exhaust gases as they interact with the ambient low-density atmosphere composed predominantly of atomic oxygen. In addition, a proposed mechanism for OH(A) excitation based upon high-velocity collisions between H_2O and O is exercised. A sequence of calculations was performed to investigate the influence of the angle of attack of the engine upon the predicted radiation levels. In general, it is found that the predicted OH(A) generation has a very large spatial scale, on the order of several kilometers. Comparison of the predictions with data showed the predictions were high, leading to speculation that the excitation cross section used in the calculations may be suspect. A preliminary variation of the energy threshold was performed using a set of experimental conditions. It was found that an increase in the energy threshold could bring the predictions into agreement with both the spatial distribution and the absolute signal level of the experimental data.

Introduction

Exoatmospheric rocket exhaust plumes present a challenging situation for accurate modeling because the rarefied reactive atmosphere interacts with the plume over very large length scales. Understanding the dynamics of exhaust plumes or jets is critical to missions such as docking maneuvers near future space stations, where the plume may impinge on critical surfaces. In addition to understanding the gas dynamics, the post-combustion reactivity of plumes is also of interest. In particular, it has been reported that visible and ultraviolet glows exist in the plume far downstream of the nozzle exit. Recently, an experimental effort was initiated to measure the ultraviolet radiation from very high altitude rocket exhaust plumes.[1,2] The concept is to use the Mir space station as a measurement platform to conduct passive radiometric observations of the rocket exhaust jets of spacecraft which supply the Mir station. As stated in Refs. 1 and 2, an ultraviolet imager aboard Mir has recorded radiation emitted from plumes in the bandpass from 280 to 320 nm. Because this radiation is robust and easily detected, the experimental effort has attempted to identify the radiator and isolate the chemical mechanism responsible for the excitation. This is intended to be the first step of a multitask process that will eventually include data acquisition on many of the UV emitters in other bandpasses.

As discussed in Ref. 2, it is surmised that the detected radiation originates from the OH(A) specie, although some contribution to the radiation may be due to NH(A). Viereck, et al., have reported considerable NH(A-X) radiation in the plume of the small VRCS US Shuttle motors, while both OH(A-X) and NH(A-X) have been identified in the larger PRCS thruster.[3] Since the instrument response curve of the current Mir UV instrumentation heavily

* The research reported herein was performed by the Arnold Engineering Development Center (AEDC), Air Force Materiel Command. Work and analysis for this research were performed by personnel of Sverdrup Technology, Inc., AEDC Group, technical services contractor for AEDC. Further reproduction is authorized to satisfy needs of the U. S. Government.

† Senior Member, AIAA.

‡ Member, AIAA.

emphasizes OH(A-X) radiation at 310 nm over NH(A-X) radiation at 337 nm, it will be presumed for the purposes of this numerical study that the dominant radiation source measured in the MirEx imagery is OH(A-X).

The authors have previously put forth a hypothesis for the excitation of OH(A), originally due to Kofsky, et al.[4] The hypothesis is that H_2O molecules are expelled from the orbiting nozzle at a relatively high velocity with respect to the "quiescent" atmosphere. Since orbital velocities are on the order of 7 to 8 km/sec, and typical plume nozzle exit velocities can be on the order of 3 km/sec, a considerable relative velocity may exist between the plume molecules and the atmospheric atomic oxygen. The largest relative velocity of the plume H_2O with the atmosphere is the case in which the motor is retrofiring. Kofsky, et al., reviewed the laboratory measurements for $H_2O + O \rightarrow 2\ OH(X)$ and reasoned that the production rate of OH(A) would be proportional to the ground-state OH production rate by a factor depending upon an activation energy. They estimated the activation energy as simply the heat of formation required to produce OH in the excited electronic state. In terms of experimental parameters, the threshold velocity to overcome the assigned activation energy is 10.45 km/sec. While this is certainly a reasonable approach, no experimental data have been recorded on the exact form of the reaction cross section for direct OH(A) production from high-energy collisions between H_2O and O.

The purpose of the present Direct Simulation Monte Carlo (DSMC) modeling of rocket exhaust plumes is twofold (1) to provide guidance for experiment planning, and (2) to assess the likelihood of possible excitation schemes. The resolution of the problem will require an iterative methodology between experiment and theory until the point is reached when the excitation and the reaction scheme can be unequivocally identified and simulated. Certainly, the combined experimental and theoretical effort has not reached this point yet, as there are many issues that are yet to be resolved. In this context, it is still very fruitful to learn the characteristics of the $H_2O + O$ reaction mechanism, and to assess the consistency of the data acquired to date with the numerical results. Clearly, if the numerical results cannot be reconciled with the data, then a different hypothesis for OH(A) excitation should be sought.

For this analysis, two data collection activities will be evaluated. Both the Progress-M and Soyuz-TM spacecraft used the same rocket motor, denoted in this report as the PME. In one case, the Progress-M underwent dedicated maneuvers, and data were acquired at near 90-deg aspect angle to the plume flow. In the second case, the Soyuz-TM crew transport undertook standard reentry procedures for retrofiring, accomplishing the 4-min duration principal burn in darkness. While the analysis will demonstrate properties of the interaction of H_2O and the ambient atomic oxygen, the purpose is to understand the spatial lengths, energy scales, and collision dynamics of the flow in general. As an aid to future experiment planning, two numerical variations are performed, one in which the angle of attack is varied, and the other as a variation of the molecular energy barrier for OH(A) production. These variations are intended to assess the $H_2O + O$ hypothesis and determine the sensitivity to experimental conditions. As a last action, the most recently acquired data will be used to compare with the absolute level of predicted OH(A) generation as a test of reasonableness of the $H_2O + O$ hypothesis.

Method

As mentioned above, the DSMC results presented here will focus on replicating, to an extent, two measurements of the PME exhaust plume. While much greater detail may be found in Refs. 1 and 2, a brief description is given here. The PME is the main thruster used in the Progress-M cargo ship and the Soyuz-TM crew transport ship. The engine uses UDMH and N_2O_4 as fuel and oxidizer, respectively, with an O/F ratio of 1.8. The nominal thrust of the PME is 3100 N (700 lbf). It has a nozzle expansion area ratio of 48. Measurements of the near-field exhaust plume radiation indicate the PME has a rapid startup.[2] The PME is quite often used to boost the Mir orbit while the Progress-M is docked. A numerical solution for the combustion and nozzle flow has been reported earlier,[1] and the nominal exit plane characteristics are shown in Table 1.

Table 1. Computed Exit Plane Gas Flow Parameters of the PME Rocket Engine

Temperature, K	698
Pressure, N/m^2	1.05×10^3
Density, molecules/cm^3	1.09×10^{17}
Velocity, cm/sec	2.99×10^5
$[H_2O]$	0.2884
$[N_2]$	0.2668
$[H_2]$	0.1905
[CO]	0.1891
$[CO_2]$	0.0531
[H]	0.0110
[OH]	1.07×10^{-5}
[O]	9.20×10^{-6}

[ ] mole fractions

In the first measurement, which occurred on 15 May 98, an unmanned Progress-M spacecraft was positioned near the Mir station for the execution of three, short duration (5-15 sec) burns. Two of the burns, denoted as dV3 and dV4, were performed such that the Progress-M plume was within the field of view of the UV imager located inside the Mir station. The details of the burns are summarized in Table 2.

Table 2. Summary of PME Retrofirings

	dV3	dV4	Reentry
Spacecraft	Progress-M	Progress-M	Soyuz-TM
Date	15 May 98	15 May 98	25 Aug 98
Duration, sec	15	5	244
Range from Mir to PME, km	3.7	9.2	15 to 28
Imager viewing angle, deg	103	84	173 to 168
Thrust-Wind angle, deg	157	176	180 to 164
PME Altitude, km	386	381	385 to 377

The second key measurement was performed on August 25, 1998, while the Soyuz-TM manned spacecraft began its initial descent to earth after having been docked to Mir on a 10-day mission. The Soyuz-TM craft dedocked from Mir and drifted to a position 15 km behind Mir and at 2-km higher altitude. The PME was ignited at that point. The retrofiring was lengthy, lasting over 240 sec. As the burn occurred, the Soyuz-TM slowed slightly and decreased altitude from 385 km to 377 km. In addition, the plume thrust vector gradually deviated from the vehicle velocity vector due to orbital mechanics at a rate of roughly 0.066 deg per second. Thus, the firing began with a 180-deg angle between the plume thrust vector and the wind vector, and finished with a 164-deg angle between the plume thrust vector and the wind vector.

The DSMC code used to model the PME flow was SOCRATES, written by Elgin, et al., in 1992 for the USAF Research Laboratory, formerly known as Phillips Laboratory.[5] The SOCRATES code was originally written to study plume contamination effects on the U. S. Shuttle produced by burns of the Shuttle motors. The code has been successfully used in the analysis of the NH(A-X) emission reported by Viereck in Ref. 3.

The underlying method of SOCRATES is based upon the work of Bird.[6] The adaptation provided by Elgin, et al., incorporates a nonuniform three-dimensional Cartesian grid. The code input allows the user to specify the desired chemistry set of interest completely. The chemical processes can be input either in Arrhenius form or as tabulations of energy and cross section. For Arrhenius rates, SOCRATES performs a standard manipulation to determine the cross section as a function of the relative velocity of the collision partners, using the variable hard sphere model. The internal energy of the molecules is taken into account by the Larsen-Borgnakke phenomenological model.[7]

Rather than perform a detailed continuum fluid dynamical analysis of the nozzle exit flow, the SOCRATES code replaces the nozzle with a point source and uses Brook's model to determine the distribution of molecules entering the solution domain.[8] This is entirely justified, since the solution domain has length scales of kilometers, while the nozzle diameter is only 0.3 m.

In the current application, a computational domain was defined which encompassed a volume of 10 km × 10 km × 13 km about the PME in the x, y, and z dimensions, respectively. The plume thrust axis is placed along the +z dimension, with the wind vector placed along the –z dimension for a full retrofiring. The domain was divided into 7168 cells, using a scheme of 16 × 16 × 28 grid planes. The SOCRATES default value of three simulated molecules per minor species per cell, and 20 simu-

lated molecules per major species per cell was used, although a variational study of these values did not appreciably affect the results. (A major species is defined to have a mole fraction within a factor of three of the maximum mole fraction in a given cell.)

SOCRATES determined the atmospheric parameters used in the current calculation, via an implementation of the MSIS '90 atmospheric model. For example, at an altitude of 383 km, the free-stream number density was determined to be 1.34×10^8 molecules-cm^{-3}. The ambient temperature was 883 K, which results in a mean free path of the undisturbed atmosphere as 2.4×10^6 cm, and a nominal collision rate for a given molecule of 1 collision per 22 secs. The molar composition of the atmosphere at this altitude is approximately 94-percent atomic oxygen, 4-percent molecular nitrogen, and 2-percent helium, although these values depend upon the solar cycle, etc.

For the present modeling, the exhaust flow was assumed to be nonreactive, with the exception of the proposed $H_2O + O$ reaction. The lack of a detailed reactive model for the near-field plume exhaust gases prohibits a close examination of the near-field flow, on the order of tens of meters, as far as OH(A) generation is concerned. That examination is left to a later work. For now, the primary task is to estimate the far-field structure of the plume and assess the plausibility of the $H_2O + O$ mechanism for OH(A) generation.

Results

As a first step, the PME flow for a nominal retrofiring was calculated. The PME exit plane properties (Table 1) were used at an altitude of 383 km. The PME was assumed to have a vehicle velocity of 7.35 km/sec, in keeping with the experimental value. The plume was directed directly into the oncoming atmospheric wind, which is composed mostly of atomic oxygen.

The predicted total number density is shown in Fig. 1 as a cut through the solution domain along the symmetry axis. The dimensions of the solution region are 13 km horizontally and 10 km vertically. The PME nozzle is located 5 km from the left side of the solution region, and is denoted by the '+.' The grid size near the nozzle exit is 240 m in the axial direction and 380 m in the other two directions. Thus, the rapid expansion of the plume gas from the initial density of 10^{17} cm^{-3} is not fully captured by this coarse resolution. The ambient density is 1.3×10^8 cm^{-3}. The outer contour in Fig. 1, marked A, indicates a density of 2×10^8 cm^{-3}, while the contour line marked B indicates a density of 2.5×10^9 cm^{-3}. The B contour is roughly 2 km downstream of the nozzle exit and provides a reasonable length scale for the far-field plume.

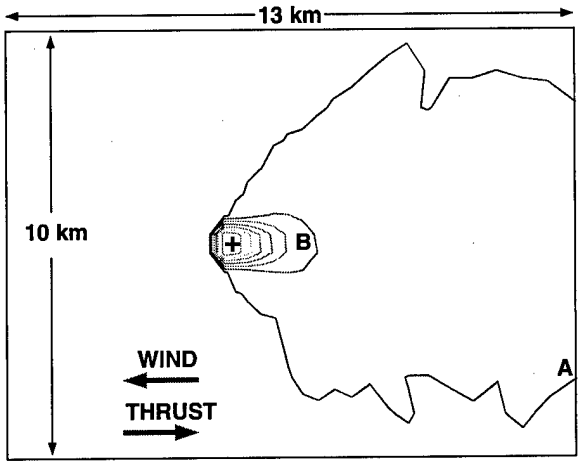

Fig. 1. Total number density in the PME retrofiring plume.

Figure 2 shows a profile of the total number density taken along the plume axis of Fig. 1. Again we note that the ambient density is ~10^8 cm^{-3}; the lower values of the number density "behind" the PME indicate that the PME plume "sweeps" the ambient atmosphere, creating a spatial region of lower density. Also shown is the gradual decay of the far-field plume density to the ambient atmospheric density.

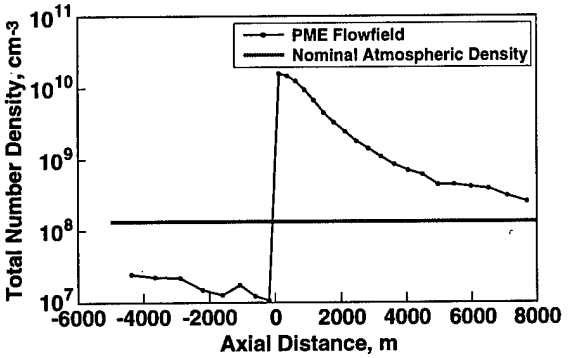

Fig. 2. Axial profile of the total number density in the PME retrofiring plume.

The density of H_2O exhausted in the plume will be proportional to the total density, since H_2O is modeled as comprising a fixed proportion of almost 30 percent of the plume. Fig. 3 displays the mean velocity of the expelled water in each computational cell. The position of the PME is denoted in the figure by a "+." The mean velocity is obtained by averaging over all H_2O molecules in a given cell, including the molecules that have undergone scattering collisions, as well as those that have not. In this context, the mean velocity provides a picture of the dominant behavior of the molecules. It must be emphasized, though, that the average velocity of a given species can be a misleading parameter when speaking of single-collision events such as the production of OH(A) from the high-energy collision of an H_2O molecule with an oxygen atom. The direction and magnitude of the mean velocity vector should not be interpreted as precluding individual molecular trajectories and collision events. The data for Fig. 3 were extracted from a slice through the center of the solution domain. The length of the vectors indicates the relative scaling of the mean velocity, while the color of the vectors corresponds to the z component of the mean velocity vector. The plume exhaust is, in general, turned back into the direction of the atmospheric wind, but over distance scales of tens of kilometers. The z velocity component along the plume axis is plotted in Fig. 4. The vacuum acceleration of the nozzle exhaust flow is noted by the increase in the H_2O velocity from the nozzle exit value of 3×10^5 cm/sec to over 3.2×10^5 cm/sec roughly 1 km downstream.

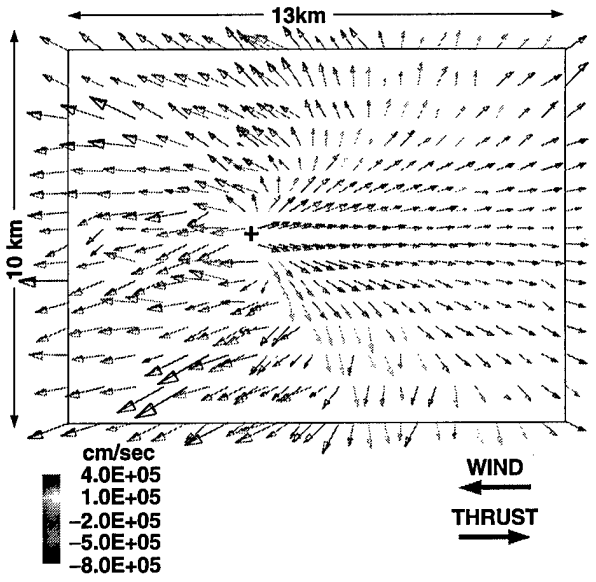

Fig. 3. H_2O average flow velocity in PME retrofiring plume, colored by average Z-component.

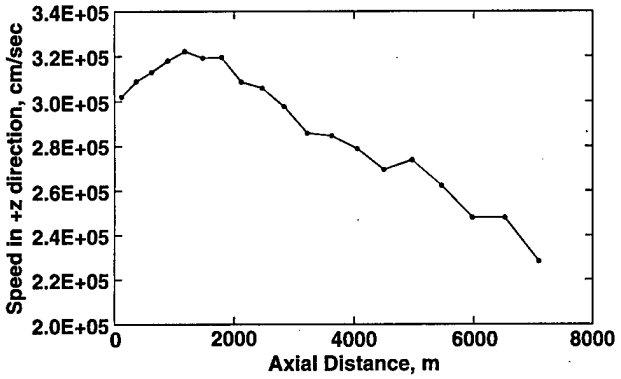

Fig. 4. Axial profile of the H_2O average Z-component of the flow velocity in the PME retrofiring plume.

An important parameter is the ambient atomic oxygen distribution, taken in the reference frame of the spacecraft. Figure 5 shows the density contours of the O-atom for the center slice through the solution domain, where the PME is denoted by the "+." The most notable feature is the depletion of O-atoms behind the spacecraft, where even after 5 km from the PME, the O-atom hole shows no sign of filling. In front of the PME one can discern a slight rise in the O-atom density, presumably due to a "snowplow" effect. It was found that the plume exhaust does not significantly alter the mean atmospheric flow direction. Of course, the individual direction of travel of those O-atoms which scatter

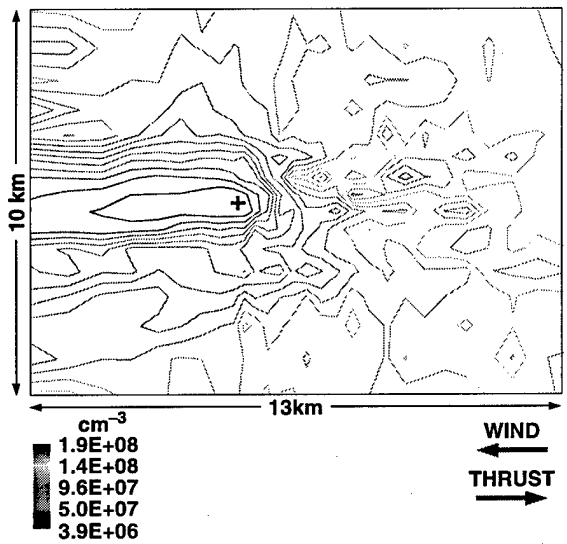

Fig. 5. O-atom number density in the PME retrofiring plume.

off the plume molecules can be radically altered as a result of the collision.

The collision frequency of atomic oxygen and H_2O is shown in Fig. 6. It is somewhat deceptive in that the contour map resembles the total density contours of Fig 1. However, the location of the PME is marked on Fig. 6 by the "+." This figure shows that the maximum in the O-H_2O collision frequency occurs nearly 1 km downstream of the PME nozzle exit.

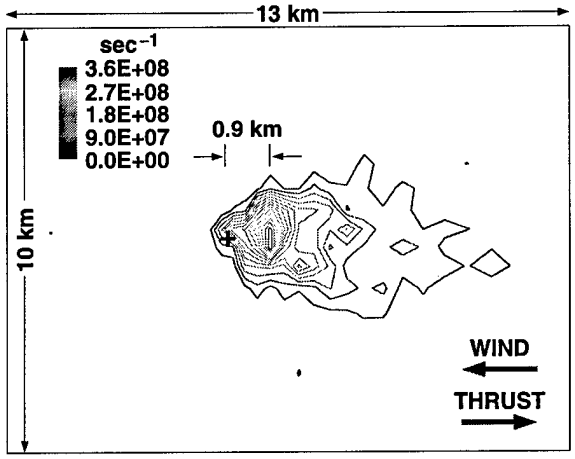

Fig. 6. Collision frequency of H_2O with O-atoms in the PME retrofiring plume.

In addition to the 180-deg thrust-wind angle, a 90-deg thrust-wind angle was to estimate the spatial scale of the flow when the exhaust is being blown sideways. Figure 7 presents the computed H_2O density contours, which will be nearly identical to the total density contours. Figure 7 shows that the rarefied atmosphere does not significantly disturb the flow direction of the PME exhaust, at least to within the first 5 km available in the computation. However, the H_2O mean flow velocity is notably distorted from the 180-deg solution, as shown in Fig. 8. In this case, the leeward side of the PME exhaust expands quite uniformly but the windward side of the mean flow velocity is not a uniform expansion. The color-coding of Fig. 8 indicates the z-velocity component for each computational cell and, as expected, only the portion of the exhaust most windward to the atmosphere will have sufficient relative velocity, on average, to overcome the OH(A) reaction threshold.

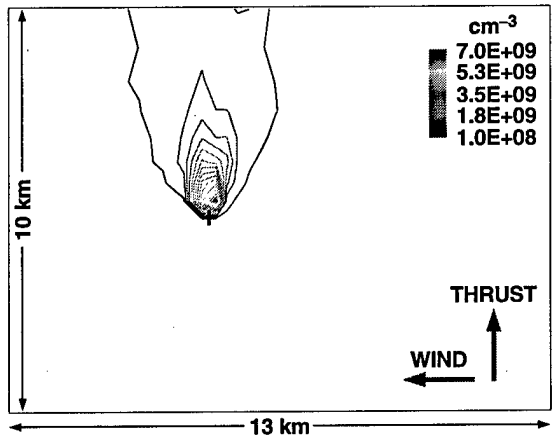

Fig. 7. H_2O number density in the PME perpendicular-firing plume.

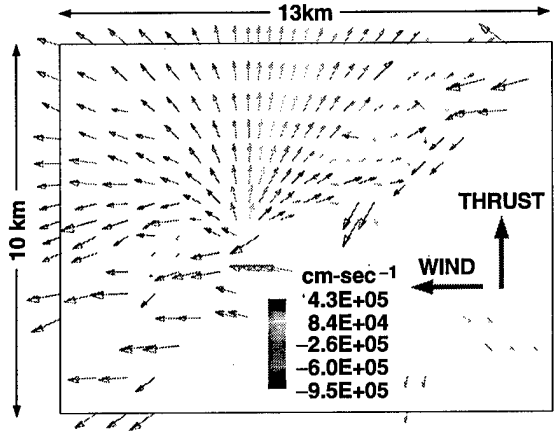

Fig. 8. H_2O average flow velocity in PME perpendicular-firing plume, colored by average Z-component.

The atomic oxygen density is shown in Fig. 9 for the 90-deg thrust-wind angle case. In this contour plot, the deficit of O atoms behind the PME plume is again apparent as in the 180-deg case of Fig. 5, but with the variation that the deficit region is stretched to shadow the entire plume. Also apparent in Fig. 9 is the excess density of O atoms on the windward side of the plume. The peak of the excess is roughly a factor of two over the ambient level. An interesting point is that the O-atom excess is not located at the nozzle exit, where the plume density is highest. Rather, it is located roughly 1.2 km from the PME nozzle exit, presumably where the optimal combination of density and spatial divergence creates the most effective "net" for collecting the fast O atoms. This is displayed in the map of the O-atom mean velocity shown in Fig. 10. The color coding again refers to the z-component of the mean velocity, and it is seen that in the region downwind of the plume, the O-atoms are

significantly slowed, and very slightly "entrained" by the exhaust flow, resulting in an upward curvature to the flow direction. The direction straightens very quickly, however, although the mean O-atom velocity downstream of the plume is much slower than the ambient value.

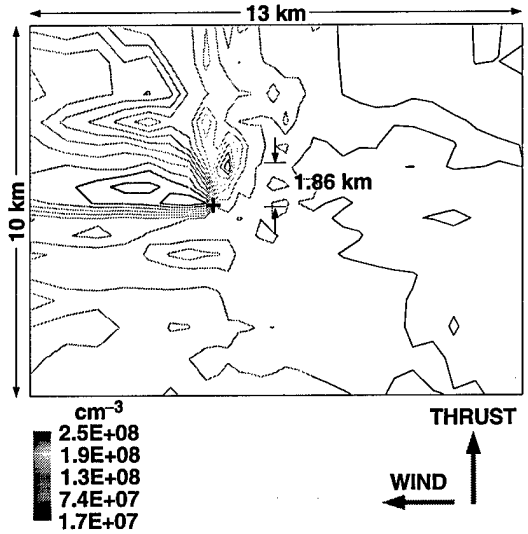

Fig. 9. O-atom number density in the PME perpendicular-firing plume.

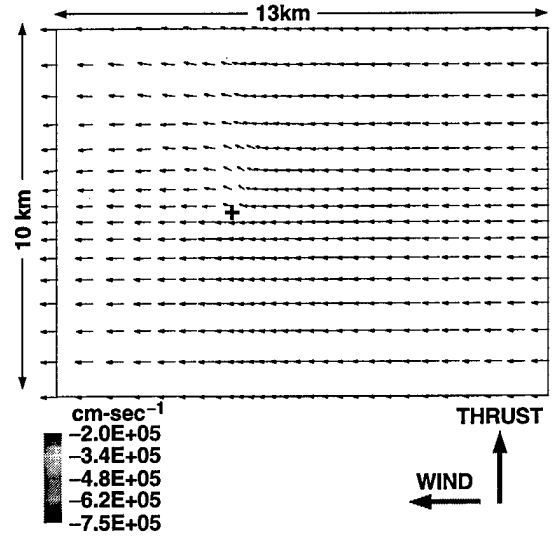

Fig. 10. O-atom average flow velocity in PME perpendicular-firing plume, colored by average Z-component.

The examination of the radiation from the PME exhaust flow is a closer comparison to the measurable data than the gasdynamic calculations. Although SOCRATES does not contain a radiative model for OH(A), it does come with a utility to construct line-of-sight summations of the flow properties. This tool is usually quite useful for predicting various emitters in the IR, such as CO_2, for which radiative models exist within SOCRATES. In this case, however, the volumetric generation of OH(A) will be sufficient to replicate the expected spatial distribution of OH(A) radiation. Since the lifetime of OH(A) is very short, 6.9×10^{-7} sec, the transport and quenching of OH(A) can be neglected, and the rate of reactions which produce OH(A) can be treated as equivalent to the rate at which OH(A) photons are emitted. Under these assumptions, it is possible to construct a two-dimensional spatial maps of OH(A) emission in equivalent units of photons-sec^{-1}-cm^{-2}.

Figure 11 is an OH(A) emission map, in units of photons-sec^{-1}-cm^{-2} obtained by integrating the solution domain along parallel lines of sight. The OH(A) excitation mechanism was assumed to be the $H_2O + O$ reaction, with an activation energy of 110 kcal/mol (equivalent to 10.45×10^5 cm/sec). This computation encompassed a solution space of 10 km × 10 km × 20 km, and the PME nozzle exit is shown in the figure for clarity. The general shape of the emission matches the expectations, given the divergence of the plume density shown in Fig. 1. Note that the peak intensity occurs on the plume centerline, roughly 2 km downstream of the nozzle. This is quite easily seen on the axial profile of Fig. 12. In that plot, the axial distance is referenced to the PME nozzle exit. The OH(A) intensity rises

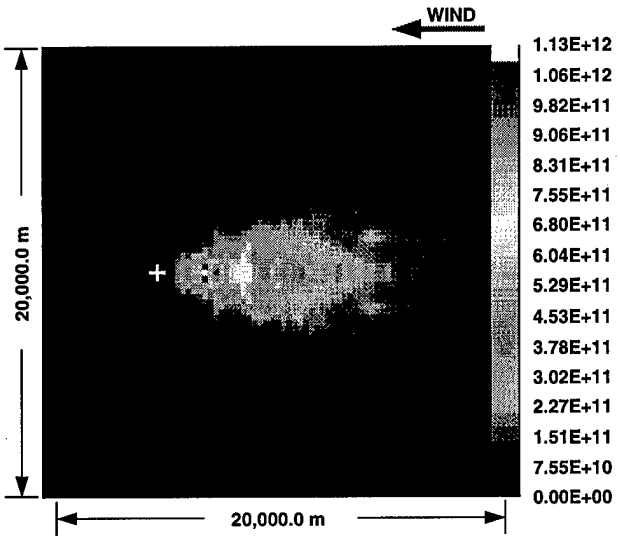

Fig. 11. OH(A) emission map produced with baseline assumptions.

over the first 2 km of plume. Downstream of 2 km, the plume intensity gradually declines in the average, but with notable oscillations. Further review with finer grid spacing will determine if the oscillations are an artifact, or a true predicted structure.

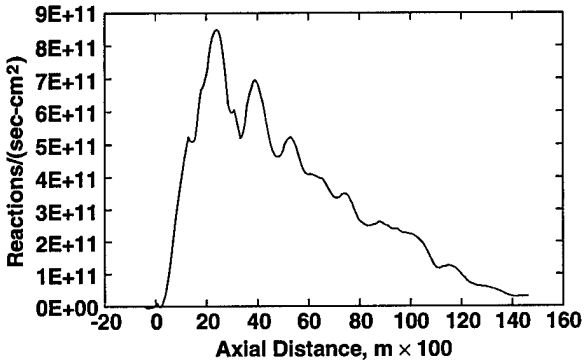

Fig. 12. Axial profile of the projected OH(A) emission map.

A key experiment variable is the emission intensity as a function of angle between the thrust vector and the wind vector. Figure 13 is a composite of ten different SOCRATES computations in which the angle between the thrust vector and the wind vector decreased from 180 to 90 degs in 10-deg increments. For each computation, the OH(A) emission map was generated from the line-of-sight projections of the solution domain. In Fig. 13, each OH(A) map has dimensions of 14 km × 14 km, although the solution domain only occupies 13 km × 10 km of that region. Furthermore, the plume thrust angle is rotating in successive images, such that the wind vector for all the images is horizontally from the right to left. The angles on the top row decrease from 180 deg to 140 deg, while the bottom row images decrease from 130 deg to 90 deg.

In the first two increments, the general shape and scale of the OH(A) emission is relatively unchanged, even though the plume thrust angle has moved from 180 deg to 170 and 160 deg. The intensity of the emission declines as the thrust angle is rotated to 150 degrees, and further to 140 degrees. However, notice that the line of maximum emission is still close to the wind vector, and not the plume thrust vector. This is in keeping with the fairly high relative velocity requirement for OH(A) production in the H_2O + O mechanism. As the thrust axis is rotated even further, we see a significant decline in the OH(A) emission, attributed to the decline in the off-axis number density of H_2O exhausting from the nozzle (see Fig. 1), and compounded by the angular variation of the exit flow velocity from the maximum along the thrust axis (see Fig. 3). Finally, for the thrust vector perpendicular to the wind vector, there is only a minor amount of OH(A) production, generated solely on the windward side of the plume. The total plume intensity is shown as a function of the thrust-wind vector angle in Fig. 14. The decline in the total OH(A) intensity, as measured in the number of reactions-sec^{-1} generating OH(A), declines by over a factor of 30 as the thrust vector rotates from retrofiring to perpendicular with respect to the wind vector due to the change in available translational energy to overcome the activation energy requirement.

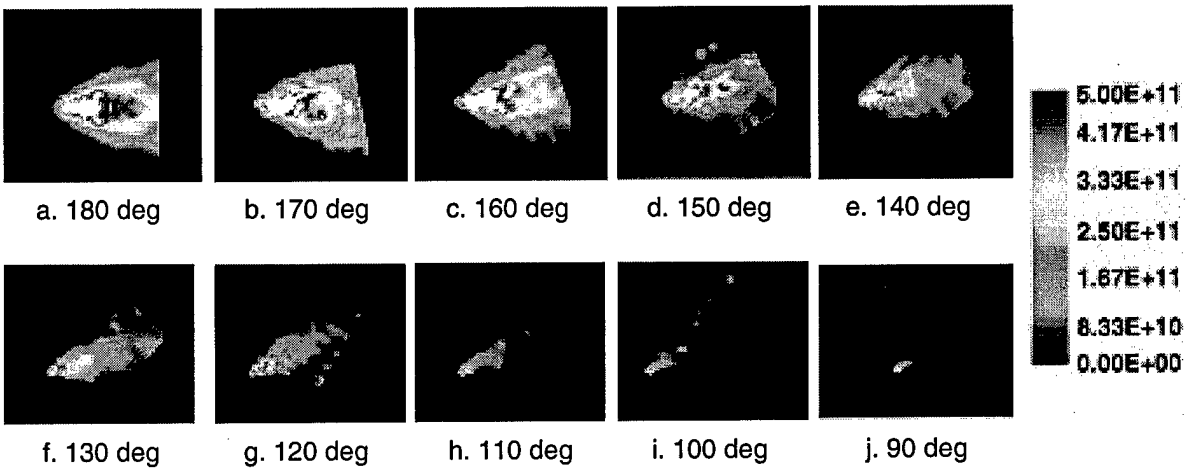

Fig. 13. Effect of angular orientation on OH(A) emission for varying angles af attack.

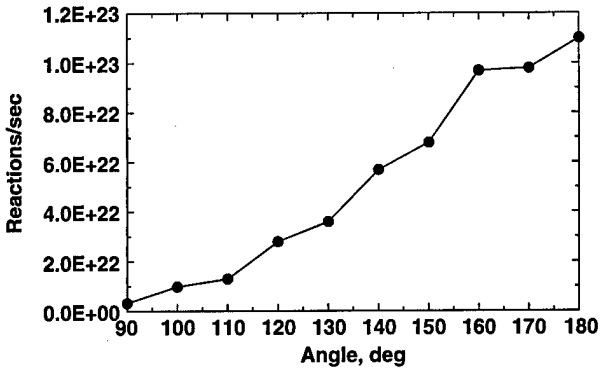

Fig. 14. Variation in total OH(A) produced as a function of the angle between the thrust and wind vector.

The preceding computations were performed using the values that Kofsky, et al., had set forth concerning the activation energy required for the OH(A) generation to proceed. The reaction rate used to this point has been,

$$H_2O + O \rightarrow OH(X) + OH(A)$$

$$k_{OH(A)} = 3.8 \times 10^{-15}\, T^{1.3}\, e^{(-Ea/kT)}$$

with E_a = 110.4 kcal/mol (4.79 eV). The prefactor value for the rate and the temperature-dependent factor are based upon a reporting of ground-state OH production by Cohen and Westberg.[10]

In an attempt to investigate the sensitivity of the production of OH(A) to this energy threshold, computations were done in which the threshold energy was varied, while the angle of attack was fixed at 180 deg. Fig. 15 shows a composite of the results for the OH(A) emission maps. As the activation energy increases, in this composite, the location of the intensity maximum moves closer to the nozzle exit as the overall intensity declines. Note that each (a), (b), and (c) have their own relative color map scales, in units of reactions-sec^{-1}-cm^{-2}. The relative change in the activation energy for each adjacent image is 0.1 eV in (a), 0.2 eV in (b), and 0.4 eV in (c). A decrease in absolute intensity of the OH(A) with increasing E_a is observed.

Figure 16 summarizes the activation energy computations by performing the spatial integrals of the OH(A) emission maps of Fig. 15. In this figure, the sharp decline in the emission of OH(A) for increasing E_a is clearly shown. It is quite interesting in Fig. 16 to observe the small rise in intensity at

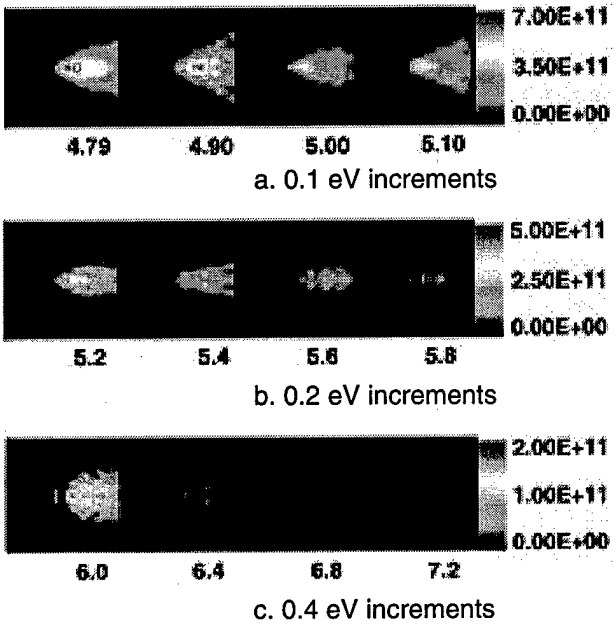

Fig. 15. Variation in the OH(A) emission as a function of activation energy.

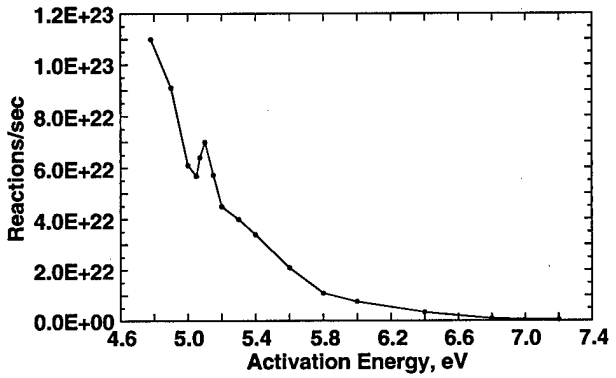

Fig. 16. OH(A) production as a function of variation in the H_2O + O reaction activation energy.

roughly E_a = 5.1 eV. Note that several additional computations were done about this feature in order to resolve it. One explanation for this peak is that as the activation energy increases, the spatial location of the intensity maximum slowly moves toward the nozzle. At 5.1eV, an optimum combination of H_2O density and O-atom density combines to give an increase in the predicted OH(A) intensity. Of course, the activation energy is a numerical not a physical, variable, and the appearance of the peak is not an experimentally useful feature. Nonetheless, the OH(A) emission level is very sensitive to the value chosen for the activation energy. For example, a 10-percent upward adjustment of the activation energy from 4.79 eV will result in a 60-percent reduction in the OH(A) produced in the flow.

At this point, a preliminary comparison to the data of August 25, 1998 can be done. Using the baseline computation conditions, i.e., E_a = 4.79 eV, and the thrust-wind vector angle = 174 deg, a predicted OH(A) distribution can be obtained which corresponds to the geometry of the measurement. The OH(A) emission map is shown in Fig 17, in which the intensity is in photons-sec^{-1}-cm^{-2}. The computational result of Fig. 17 has spatial dimensions of 10 km × 10 km. The image data acquired from the Mir station on August 25, 1998 at the start of the Soyuz-TM reentry burn have an angular dimension of 8 deg, at a range from the Mir of 15 km. A typical data image is shown in Fig. 18 for comparison with the prediction of Fig. 17. The data image has been enhanced so that the bright region corresponding to the intense near-field radiation is saturated, while the far-field luminous region is evident across the circular, active portion of the image. Note that a rough estimate of the spatial dimension of the active portion of the image, i.e. the circular region within the image, has a diameter on the order of 2 km. As noted in much more detail in Ref. 2, the estimated power emitted by the PME plume within the UV imager field of view is ~180 W. Note that the contribution of the near-field radiation to the total value is less than a percent. The radiated power corresponds to an emission of approximately 3 × 10^{20} photons/sec. Restricting the spatial integration of the predicted plume shown in Fig. 17 to an area roughly 2 km in diameter results in a predicted value of 3 × 10^{22} photons-sec^{-1}, which is two orders of magnitude higher than the observation. Even allowing for a reasonably high uncertainty in the measured data, the current reaction mechanism will overestimate the radiation either due to a cross section which is too large, or failures in the model such as collisional quenching of OH(A), or its implementation, such as inappropriate grid cell sizes, to replicate the true flow character.

One speculative explanation for the overprediction is the presence of an energy barrier to the reaction. As noted above, the production of OH(A) is rather sensitive to the value used. For example, the solution that had an activation energy of 6.8 eV was manipulated to produce a map with the August 25. 1998 measurement viewing parameters. The result was that the predicted emission was 2 × 10^{20} OH(A) emitted photons-sec^{-1}, which is in fair agreement with the data, considering the rough order of magnitude approximations used.

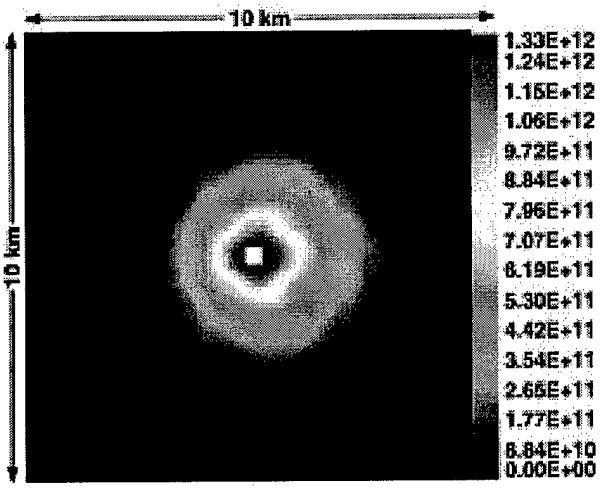

Fig. 17. Predicted OH(A) emission for August 25, 1998 Soyuz-TM reentry burn, with E_a = 4.8 eV.

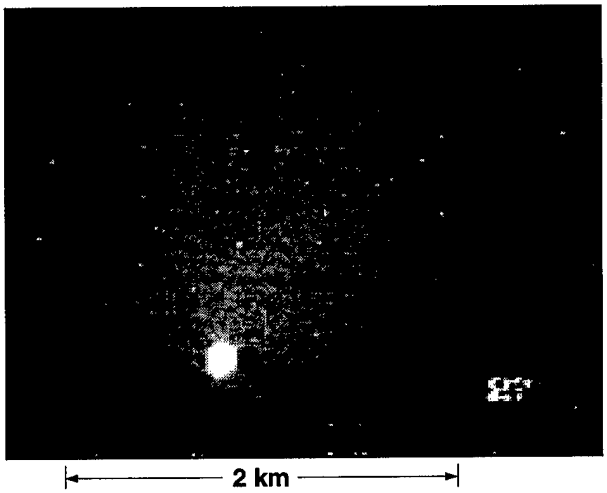

Fig. 18. Image of Soyuz-TM PME plume acquired from Mir Station during August 25, 1998 PME operation.

Discussion

This analysis has attempted to provide the framework for experimental data analysis and future experiment planning. The global flow parameters were examined, characterized by H_2O for the plume exhaust. The rarefied atmosphere, composed almost totally of atomic oxygen (as predicted by the MSIS'90 model), permits the PME exhaust plume to extend over a distance several kilometers long. The PME disturbs the ambient

environment to a great extent, causing the depletion of the atomic oxygen behind the plume by an order of magnitude. This was true regardless of the orientation of the plume with respect to the wind vector, as demonstrated in calculations of ram and perpendicular firings.

A predicted OH(A) emission map was generated for a retrofiring PME on the basis of the hypothesized H_2O + O reaction mechanism. That result indicated the maximal plume radiation occurs downstream of the nozzle exit by 1 to 2 km. This is consistent with the previous preliminary modeling done at 350 km altitude in Ref. 1. However, the predicted far-field radiation is higher than the measured data by a considerble amount.

The overprediction of the OH(A) emission using the baseline activation energy is not inconsistent with the H_2O + O mechanism. An underprediction of the radiation would cast doubt upon the mechanism, since the SOCRATES model is an idealistic case as it lacks potential quenching and radiative effects. While these effects are expected to be small, they will lessen the prediction. Ideally, a closer result would be desirable; however, the overprediction is likely due to an overestimate of the reaction cross section, i.e., the rate constant. The H_2O + O reaction equation contains three parameters in the expression of the rate constant; the prefactor, the temperature exponent, and the activation energy. As a first look into the effect of uncertainty in the rate constant, an assessment of the OH(A) production with varying activation energy was done for a retrofiring PME plume. Recall the origin of the rate constant expression as being the electronic ground-state reaction rate expression, with the activation energy replaced by the enthalpy of the excited state products. Assuming that the prefactor and the temperature exponent describe the measured dynamics of the H_2O + O ground-state collision system, it is not unreasonable to consider the activation energy as a source of uncertainty for the electronically excited system.

Computations of the electronically excited interaction hypersurfaces of H_2O and O may be used to confirm or reject the concept of an activation energy barrier to the production of OH(A) and OH. Furthermore, such a computation would be able to provide a prediction on the other factors in the rate constant expression, as well as insight on the expected form and distribution of the internal energy of OH(A). This could then be tested against calibrated spectra obtained in future MirEx tests.

Acknowledgments

The authors wish to acknowledge the support of the U. S. Air Force Research Laboratory, especially the U. S. Air Force Office of Scientific Research, for support of this effort.

References

1. Karabadzhak, G. F., Plastinin, Yu, Khmelinin, B. Teslenko, V., Shvets, N. Drakes, J. A., Swann, D. A., and McGregor, W.K., "Experimentation using the Mir Station as a Space Laboratory," AIAA Paper 98-0288, 36th AIAA Aerospace Sciences Meeting & Exhibit, Reno, NV, January 1998.

2. Karabadzhak, G. F., Plastinin, Yu, Afanasiev, A., Szhenov, E., Drakes, J. A., McGregor, W. K. Bradley, D., Teslenko, V., Shvets, N., Volkov, O., and Kukushkin, V., "Measurements of the Progress-M Main Engine Retrofiring Plume at Orbital Conditions," AIAA Paper 99-1042, 37th AIAA Aerospace Sciences Meeting & Exhibit, Reno, NV, January 1999.

3. Viereck, R. A., Murad, E., Knecht, D. J., Pike, C. P., Bernstein, L. S., Elgin, J. B., and Broadfoot, A. L., *J. Geophys. Res*, Vol. 101, 1996, p. 5371.

4. Kofsky, I. I., Barrett, J. L., Brownrigg, T. E., McNicholl, P. N., Tran, N. H., and Trowbridge, C. A., "Excitation and Diagnostics of Optical Contamination in the Spacecraft Environment," AFGL-TR-88-0193, July 1988.

5. Elgin J. B. and Bernstein, L. S., "The Theory Behind the SOCRATES Code," PL-TR-92-2207, August 1992.

6. Bird, G. A., Molecular Gas Dynamics and the Direct Simulation of Gas Flow, Oxford University Press, New York, 1994.

7. Borgnakke, C., and Larsen, P. S., *J. Computational Physics*, Vol. 18, 1975, p. 405.

8. Brook, J. W., *J. Spacecraft and Rockets*, Vol. 6, 1969, p. 626.

9. Cohen, N. and Westberg, K. R., *J. Phys. Chem. Ref. Data*, Vol. 12, 1983, p. 531